Direct Visualization of Spruce Budworm Antifreeze Protein Interacting with Ice Crystals: Basal Plane Affinity Confers Hyperactivity

Natalya Pertaya,* Christopher B. Marshall,† Yeliz Celik,* Peter L. Davies,† and Ido Braslavsky*
*Department of Physics and Astronomy, Ohio University, Athens, Ohio; and †Department of Biochemistry, Queen's University, Kingston, Ontario, Canada

ABSTRACT Antifreeze proteins (AFPs) protect certain organisms from freezing by adhering to ice crystals, thereby preventing their growth. All AFPs depress the nonequilibrium freezing temperature below the melting point; however AFPs from overwintering insects, such as the spruce budworm (sbw) are 10–100 times more effective than most fish AFPs. It has been proposed that the exceptional activity of these AFPs depends on their ability to prevent ice growth at the basal plane. To test the hypothesis that the hyperactivity of sbwAFP results from direct affinity to the basal plane, we fluorescently tagged sbwAFP and visualized it on the surface of ice crystals using fluorescence microscopy. SbwAFP accumulated at the six prism plane corners and the two basal planes of hexagonal ice crystals. In contrast, fluorescently tagged fish type III AFP did not adhere to the basal planes of a single-crystal ice hemisphere. When ice crystals were grown in the presence of a mixture of type III AFP and sbwAFP, a hybrid crystal shape was produced with sbwAFP bound to the basal planes of truncated bipyramidal crystals. These observations are consistent with the blockage of c-axial growth of ice as a result of direct interaction of sbwAFP with the basal planes.

INTRODUCTION

Many organisms are protected from freezing by antifreeze proteins (AFPs), which adsorb to ice, modify its morphology, and prevent its further growth (1–4). AFPs were first found in fish, which have a rich diversity of AFP types (5), and subsequently in arthropods (6,7), plants (8,9), bacteria (10,11), and fungi (12). By protecting their hosts from freezing, AFPs contribute greatly to the biodiversity and productivity of ecosystems at high altitudes and latitudes. They have applications in diverse areas, including agriculture (e.g., protecting crops from frost) (13–18), aquaculture (e.g., protecting transgenic fish against freezing) (19), and in medicine (e.g., cryosurgery and cryopreservation). Moreover the ability of AFPs to influence crystal growth suggests that they might serve as a model system for the study of biomineralization and also might play a role in future nanotechnology applications. For all these reasons, it is important to understand how AFPs function.

The generally accepted ''adsorption-inhibition'' (1,20–22) mechanism for AFP activity proposes that the specific binding of these proteins to an ice surface results in the inhibition of ice growth through the Gibbs-Thomson effect (20). The binding of the protein to the surface is principally the result of the entropic effects of docking a relatively hydrophobic, flat protein surface to ice, as well as van der Waals contacts and the formation of some hydrogen bonds (1,23–25). The ice surface is pinned by the adsorbed AFPs and forms curved microsurfaces between the bound proteins that limits further growth of the ice (21,26). As a result, the nonequilibrium freezing temperature is lowered below the melting point, and, within this thermal hysteresis (TH) gap, the ice crystals appear to be stable (as judged by light microscopy), neither growing nor melting over several days (27). Such ice crystals usually have a characteristic faceted morphology that is formed due to the inhibition of the growth of the crystal planes to which the AFP binds. This has been most convincingly shown for the type I AFP from winter flounder, for which both the binding plane and the direction of binding have been determined using an ice etching technique (28). In this method a single crystal hemisphere is grown in an AFP solution and then allowed to partially sublimate. After sublimation, regions of the hemisphere to which AFPs bound are shown by the texture of the surface, which is affected by the presence of the AFP. In the experiments on the type I AFP from winter flounder (28), the binding plane defined a hexagonal bipyramidal crystal with a predicted *c*/*a* axial ratio of 3.3:1, a result that has been consistently obtained for this AFP (29). Other fish AFPs, such as the type III AFP from ocean pout (AFPIII), produce hexagonal bipyramidal crystals with a more variable morphology. For this AFP, the crystal axial ratio is affected both by dilution and by mutation of surface residues, possibly because this type of AFP can bind to more than one ice plane (30).

Terrestrial insects, which are exposed to more extreme temperatures than aquatic organisms, exhibit higher TH activities in their body fluids than do fish. However, it was not until insect AFPs were purified to homogeneity that their exceptional specific activity was fully appreciated (31). Whereas fish AFPs, at circulating concentrations of 10–20 mg/mL, produce TH activities of ~0.5–1C°, insect AFPs depress the freezing temperature by 4–5C° at one tenth of this concentration (31–33) (Fig. 1 *A*). For this reason, insect AFPs were termed ''hyperactive'' (31). Subsequent to their identi-

Submitted November 20, 2007, and accepted for publication February 28, 2008.

Address reprint requests to Ido Braslavsky, Dept. of Physics and Astronomy, Ohio University. Tel.: 740-597-3011; E-mail: braslavs@ohio.edu.

Editor: David W. Piston.

0006-3495/08/07/333/09 $2.00

doi: 10.1529/biophysj.107.125328

fication in insects, hyperactive AFPs have been isolated from fish (34–36), a primitive arthropod (7), and an Antarctic bacterium (37). These AFPs, which have radically different structures from one another, have been studied for clues to their superior activity. Although they each direct the formation of ice crystals with distinct and reproducible morphologies (variously described as hexagonal plates, lemons, spindles, rice grains, or amorphous), when the freezing point is exceeded these ice crystals behave in a remarkably similar manner: They each grow explosively in directions perpendicular to the *c* axis (32,33,36,37). By contrast, the bipyramidal ice crystals formed in the presence of any one of several different types of moderately active fish AFPs grow explosively in directions parallel to the *c* axis (33).

Scotter et al. (33) proposed that the key to understanding the mechanism of AFP hyperactivity is that hyperactive AFPs hinder growth along the *c* axis. It was suggested that such protection could be achieved either by direct binding to the basal plane (perhaps explaining the large basal plane facets seen in a sbwAFP-bound ice crystal) or by minimizing the radius of curvature at an exposed basal plane (as suggested by the sharp tips of the spindle produced by hyperactive flounder AFPs). To test the hypothesis that sbwAFP binds to the basal plane of ice, we attached a green fluorescent protein (GFP) to sbwAFP (Fig. 1 *B*) and directly visualized the binding of the fluorescent GFP-sbwAFP molecules to ice crystals. SbwAFP has a rigid, left-handed, beta-helical structure with a triangular cross-section stabilized by disulfide bonds (38–41). This scaffold supports an ice-binding face comprised of a two-dimensional array of threonine (Thr) residues with exquisite complementarity to the surface of the prism plane of the ice lattice; see Fig. 4 in Graether et al. (39) and Fig. 4 in Scotter et al. (33) for the structure of ice and the definition of the basal and prism planes. Thr residues on adjacent β-strands are 4.5 Å apart and the two Thr side chains within a strand are separated by 7.35 Å. These dimensions match the spacing of O atoms on the prism plane (4.5 × 7.35 Å) almost perfectly, and are a close fit to the spacing of O atoms on the basal plane (4.5 × 7.8 Å). Although it is clear that the ice lattice matching of insect AFPs is important for antifreeze activity, the details of the mechanism that mediates binding are not known. An early 'ice lattice occupation' model proposed that Thr side chain hydroxyl groups occupy lattice positions, essentially 'freezing' onto the ice surface (42). Although this model can be adapted to fit the insect AFPs into the lattice (43), a subsequent binding model docked both the hydroxyl and methyl groups of the Thr array into cavities on the ice surface (40). The latter model enabled the formation of extensive van der Waals interactions needed for the hydrophobic effect, while allowing the formation of some hydrogen bonds. Binding mechanisms that rely solely on hydrogen bonding suffer from the criticism that hydrogen bonds to the solvent (water) are thermodynamically favored over those made to ice (24). The importance of the hydrophobic effect in binding AFPs to ice is that constrained water can be released from both ice and the hydrophobic ice-binding site of the AFP resulting in an appreciable gain in entropy (23). Note that hydrogen bonds within the hydrophobic contact zone are insulated from contact with the solvent and can contribute to the binding interaction (44).

As a control we also studied a GFP-labeled moderately active fish AFP, namely AFPIII, which is a 7-kDa globular protein with a beta-clip fold (Fig. 1 *C*) (45,46). Using fluorescence microscopy as well as macroscopic single crystal ice hemispheres, we were able to directly visualize the binding of both fish and insect AFPs to ice crystals. Our results indicate clearly that sbwAFP (but not AFPIII) binds to the basal plane. Furthermore, ice crystals exposed to a solution containing a mixture of the two AFPs exhibited hybrid morphology, namely a modified bipyramidal ice crystal with truncated tips where small but well-defined basal plane facets were coated with sbwAFP.

MATERIALS AND METHODS

Experimental equipment

The experimental system has been described previously (4,47). In brief, the sample is held between two glass coverslips. A 22-mm square coverslip is used as the base of the cell onto which a drop (~4 μl) of AFP solution is placed. An 18-mm circular coverslip placed on the liquid is used as the top of the cell. The depth of the liquid layer in the cell is not controlled and is typ-

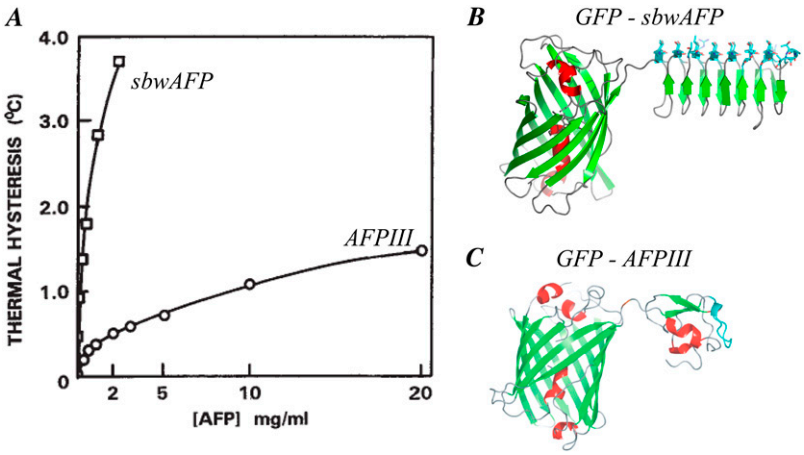

FIGURE 1 AFP-GFP conjugates. (*A*) Thermal hysteresis versus concentration for fish AFP type III (AFPIII) and insect spruce budworm antifreeze proteins (sbwAFP). (*B*) Ribbon diagram of sbwAFP linked to green fluorescent protein (GFP). (*C*) Ribbon diagram of AFPIII linked through its N-terminus to the C-terminus of GFP. The light blue region is the ice binding site. The α-helices are shown in red and the beta-strands in green. Figure assembled with modifications from (*A*) Tyshenko et al. (32), (*B*) Pertaya et al. (47), and (*C*) Pertaya et al. (4).

ically 10–15 μm. Uncured polydimethylsiloxane (PDMS) is used to seal the periphery of the coverslip to avoid evaporation of the solution. The coverslips are placed on a temperature controlled metal plate that contains an array of fine holes with a diameter of 125 μm. These holes allow light to illuminate the sample but are fine enough to minimize temperature gradients in the sample. The sample is imaged with a confocal fluorescence microscope (ZEISS LSM 510) equipped with illumination (488 nm Argon laser line and 543 nm and 633 nm HeNe laser lines), and filters for the detection of eGFP (48), monomeric orange fluorescent protein (mOrange) (49), and Cyanine 5 (Cy5).

Expression and purification of the GFP labeled AFPs

The construction, and expression of the GFP-AFPIII gene, as well as the isolation and purification of its protein product, are detailed in Pertaya et al (4). A variant encoding a mOrange–AFPIII fusion protein was cloned and produced by similar methods. mOrange was obtained from Dr. R.Y. Tsien (University of California, San Diego, CA) (49). A gene encoding eGFP-tagged spruce budworm AFP (GFP-sbwAFP) was constructed in a similar manner (47). The sbwAFP isoform 501 (41) was selected to produce this construct because it has been shown to refold more efficiently than the shorter isoforms that have been characterized. Following the example of the GFP-AFPIII construct, eGFP was linked to the N-terminus of sbwAFP via a GlyAlaGly tripeptide linker. Recombinant GFP-sbwAFP was expressed in *Escherichia coli* BL21(DE3), refolded from the insoluble fraction (41), recovered by ice affinity purification (50), and concentrated by centrifugation in an Amicon ultracentrifugal filter device (Millipore, Billerica, MA) (47).

Ice hemisphere

A single ice crystal was grown from degassed ddH_2O (MilliQ) and mounted on a cold finger to seed the growth of a single crystal hemisphere from ddH_2O (22,28). The *c* axis was oriented normal to the cold finger. This hemisphere was then immersed in a solution of GFP-AFP type III (~0.1 mg/ml in 20 mM ammonium bicarbonate) in an insulated cup and the temperature of the cold finger was gradually lowered at a rate of −0.1°C/h to effect ice growth. The hemisphere was removed from the solution before the ice grew to the edges of the cup, and allowed to melt back slightly at room temperature to remove nonspecifically bound protein. The ice was illuminated with an ultraviolet (UV) lightbox and photographed.

RESULTS

Antifreeze proteins tagged with fluorescent proteins

To visualize the location of AFP adsorbed to ice, we produced recombinant fusion proteins consisting of GFP linked to sbwAFP (Fig. 1 *B*) (47), GFP linked to AFPIII (Fig. 1 *C*) (4) and mOrange linked to AFPIII (not shown). In all constructs the N-terminus of the AFP was linked to the C-terminus of the GFP. The TH activity and ice-shaping properties of these fusion proteins are not negatively affected by the tag (51), validating the use of these recombinant proteins to directly observe AFPs bound to ice.

Visualization of antifreeze proteins on ice crystals

To visualize sbwAFP bound to ice, a thin layer of the AFP solution sandwiched between two coverslips was rapidly frozen and then melted back slowly until separate, single-crystal grains ~10–20 μm in diameter were present. In these experiments many of the larger ice crystals come into contact with the glass coverslips, altering their morphology and AFP binding characteristics (e.g., the large crystals in the upper left of Fig. 2); these crystals were not used in the assessment of binding planes. Crystals smaller then the height of the cell tend to move by Brownian motion or drift with local solution flow. Such crystals were rarely used in this study; an example of such a crystal is shown in Supplementary Material, Movie S1 and Data S1. Crystals 10–15 μm in height (approximately the same distance as the separation between the slides) touched the slides and were held in place by this interaction. The small crystals, which were barely influenced by the coverslips, took the form of hexagonal prisms and maintained this morphology during cooling within the TH gap (Fig. 2). The GFP-sbwAFP fusion proteins were present both in solution and on the surfaces of the ice crystals. Ice crystals with two different orientations were observed: crystals with sixfold symmetry (hexagonal form) have the *c* axis normal to the image plane (Fig. 2 *A*), and crystals with the *c* axis within the image plane that appear occasionally to have fourfold symmetry (Fig. 2 *B*). However, the fourfold symmetry of this latter crystal type does not represent crystallographic symmetry; rather, the observed structure is merely a projection of a tilted hexagonal crystal. The three-dimensional shape of the crystals can be better appreciated in Fig. 2 *C*, which shows that the crystals are hexagonal bifrusta with relatively undecorated pyramidal planes. The patterns of

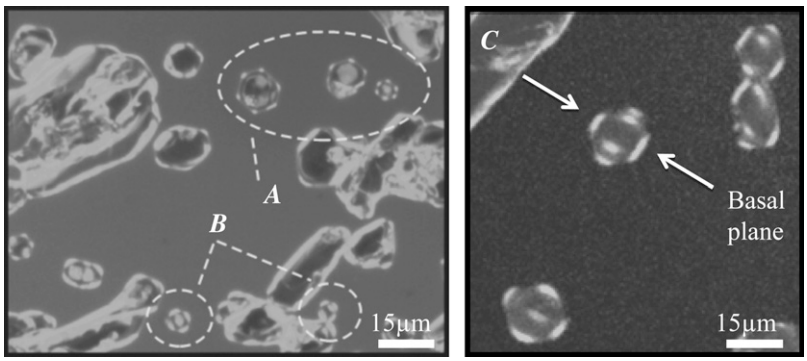

FIGURE 2 Ice crystals formed in the presence of GFP-sbwAFP. (*A*) Hexagonal ice crystals with sixfold symmetry decorated with GFP-sbwAFP. Here the *c* axis is normal to the image plane. (*B*) Crystals with the *c* axis in the image plane exhibit fluorescence that appears to have fourfold symmetry. However, this does not represent crystallographic symmetry; the observed structure is merely a projection of a tilted hexagonal crystal (Figs. 2 *C* and 3). (*C*) Additional crystals from a separate experiment where the three-dimensional crystal shape is evident. The basal planes, indicated by arrows, are separated by 15 μm. Images were taken with a confocal microscope through a 488 nm filter to visualize GFP.

fluorescence clearly show GFP-sbwAFP bound to the two polar apices of the crystal and to the six corners of the hexagonal equator. Considering the symmetry of the ice lattice, these polar surfaces must be the basal planes. Schematic interpretations of these orientations are shown in Fig. 3. The fluorescence microscopy measurements provide a unique insight into where sbwAFP binds to ice; in particular, the data can be used to determine whether the basal plane is decorated with sbwAFP. Indeed, all of the small crystals show the accumulation of sbwAFP on the basal planes, which is most evident when viewed with the *c* axis in the image plane such as in Fig. 2 *C*.

When a solution of GFP-labeled AFP type III is rapidly frozen at low temperature, ice grows as fine needles that become heavily coated with the fluorescent protein. As the ice is melted back to isolate individual crystals, the fluorescent AFP III is retained within the original core (4). The newly formed bipyramidal surfaces that emerge under moderate supercooling become coated with additional AFPs (Fig. 3 *D*). This contrasts with the behavior of crystals formed in the presence of GFP-sbwAFP, which accumulate the fluorescent signal on discrete surfaces of the hexagonal ice crystal and do not have a bright core.

Binding of AFPIII to a single crystal ice hemisphere

The microscopic ice crystals formed in the presence of AFPIII are hexagonal bipyramids in which the basal planes would only be exposed where the pyramidal planes converge into tips (Fig. 3 *D*). These basal plane surfaces are too small to permit the use of confocal microscopy to determine whether GFP-AFP III is present. Therefore, to show the lack of AFPIII binding to the basal planes, we adapted the ice hemisphere experiments of Knight et al. (28) to use fluorescently tagged type III AFP, which can be seen directly. Thus the hemisphere need not be 'etched' by sublimation. In these experiments, the hemisphere was seeded with a single crystal grown from pure water (in the absence of AFPs), then grown in a solution of GFP-AFPIII. When viewed under UV light in the direction of the *c* axis, a fluorescent band can be seen around the periphery (Fig. 4 *A*), representing the GFP-AFPIII bound to the prism and/or pyramidal surfaces. The core of the hemisphere, which was grown in the absence of AFPs, is clear and the basal plane facing the camera shows no appreciable fluorescence. When the crystal is rotated laterally by 90°, the *c* axis becomes parallel to the plane of the page (Fig. 4 *B*) and the green areas represent a view through the pyramidal surfaces that have accumulated GFP-AFP as the hemisphere was growing in the AFP solution. These results confirm those established by ice etching (28,30) and show that type III AFP does not bind to the basal planes of ice.

Dynamics of the accumulation of spruce budworm antifreeze protein on ice

To monitor the coverage and dynamics of accumulation of sbwAFP on ice crystals, we observed ~15-μm-diameter ice crystals in the presence of the GFP-tagged sbwAFP using an epi-fluorescence microscope (Nikon TE2000-U). Fig. 5 shows the behavior of one such crystal; this crystal is in the same orientation as that shown in Fig. 3 *B*. During melting, the ice crystal does not show any fluorescence (Fig. 5, *A* and *B*). However, when the temperature is lowered to just below the melting point (in the TH gap), the ice crystal stops melting and stabilizes, and GFP-sbwAFP begins to accumulate on the basal and prism surfaces (Fig. 5, *C–E*). When the temperature is lowered further, the crystal grows rapidly perpendicular to the *c* axis. The expanding ice from the ''burst'' is dark relative to both the original crystal and the surrounding solution, indicating that sbwAFP is not efficiently included into the bursting crystal. Furthermore, the solution adjacent to the

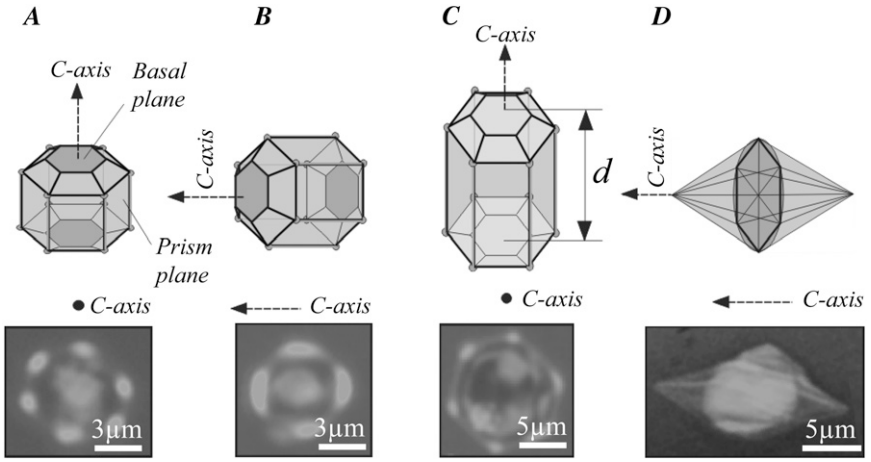

FIGURE 3 Interpretation of ice crystals formed in the presence of GFP-labeled AFPs. (*A*) A schematic interpretation of the crystal axes and main facets of a hexagonal prism crystal decorated with spruce budworm antifreeze protein. This case shows an ice crystal whose length is smaller than the distance **d** between the two coverslips, allowing the basal planes to become decorated with GFP-sbwAFP. (*B*) An ice crystal oriented with its *c* axis in the plane of the page. The basal planes at the left and right edges are brightly decorated. (*C*) An ice crystal whose length is equal to the distance **d** between two coverslips, which block the basal plane from being decorated with GFP-sbwAFP. (*D*) A diagram of a typical hexagonal bipyramidal ice crystal produced by AFPIII, illustrating that the vertices of the crystal lie along the *c* axis. In each diagram, faint AFP decoration in marked with light gray, bright decoration is marked with dark gray and areas with no GFP-AFP bound are gray. A GFP filter image (confocal microscopy) of representative ice crystal is given below each diagram.

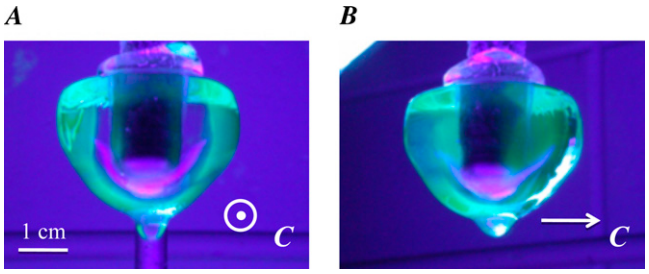

FIGURE 4 Cold finger experiment. A single ice crystal was grown from ddH_2O and mounted on a cold finger to seed the growth of a single crystal hemisphere in a solution of GFP-AFPIII (as described by Knight et al. (28)). The *c* axis was oriented normal to the cold finger and is normal to the figure plane in *A* and parallel to the figure plane in *B*. This seed was then immersed in a solution of GFP-AFPIII (see Materials and Methods) and the temperature of the cold finger was gradually lowered to effect the slow growth of the seed into a hemisphere. The hemisphere was then removed from the solution and photographed under UV illumination.

burst is brighter because the GFP-sbwAFP is being concentrated at the edge of the rapidly advancing ice/liquid interface due to its exclusion from the ice. However, the original decorated crystal is recognizable entombed within the new ice (Fig. 5 *G*), see also Fig. 5 in (47). The pattern of fluorescence and the explosive growth of the ice crystal when the freezing temperature is exceeded (Fig. 5, *F* and *G*) confirm the orientation of the *c* axis for this particular example as ice crystals in the presence of sbwAFP typically grow in a direction perpendicular to the basal orientation (33) (Movie S1 and Data S1). Additionally, a confocal image of decorated crystal and its burst are shown in Fig. 6 (see also Movie S2 and Data S1). After the burst of the crystal, the temperature was increased to stop the growth of the ice and then reduced slightly again, allowing the GFP-sbwAFP to accumulate on the ice crystal.

Stabilization of the basal planes using a mixture of AFPIII and sbwAFP

In the search of further evidence supporting basal plane binding by sbwAFP, we examined the ice-binding behavior of a mixture of differentially tagged sbwAFP and AFPIII. To allow both AFPs to contribute to ice-binding and crystal morphology, we prepared a solution in which the concentration of each AFP alone would produce 150 mOsm of TH activity. This required 0.5 mg/ml AFPIII and 0.07 mg/ml sbwAFP; note that the AFPIII is at a sevenfold higher concentration (~10-fold on a molar basis). The total TH activity in this solution was 150 mOsm; hence there was no potentiation of activity when the two types of AFP were mixed. To distinguish the two protein types when bound to the same crystal, sbwAFP was tagged with GFP (as before), and AFPIII was tagged with the mOrange version of red fluorescent protein (49). The GFP-sbwAFP and mOrange-AFPIII were visualized by alternately viewing with 488 nm and 543 nm laser illuminations, respectively. The ice crystals formed in the mixture of the fish and insect AFPs had a morphology that varied with the relative concentration of the two AFP types. At the transition from the bipyramidal shape in the presence of AFP III (Fig. 3 *D*) to the typical hexagonal shape in the presence of sbwAFP (Fig. 3 *A*), a hybrid shape in the form of a truncated hexagonal bipyramid emerged (Fig. 7). The underlying shape is that of the hexagonal bipyramid observed in the presence of AFPIII alone. However, the GFP-sbwAFP truncates the bipyramidal tips and forms small flat basal planes at both ends of the crystal (hexagonal bifrustra) that are decorated heavily with GFP-sbwAFP. No orange fluorescence is detectable at these facets, indicating that AFPIII does not bind to the basal plane in these mixing experiments.

DISCUSSION

By observing the manner in which ice crystals grow when cooled below the nonequilibrium freezing temperature, we noted that the hyperactive sbwAFP directs ice crystal growth explosively normal to the *c* axis. In contrast, the moderately active AFPIII directs the ice crystal growth along or parallel to the *c* axis. We proposed that this can be explained by the binding of sbwAFP to the basal planes of ice to prevent growth in the *c*-axial direction. By attaching fluorescent tags to these two types of AFP, we were able to directly visualize

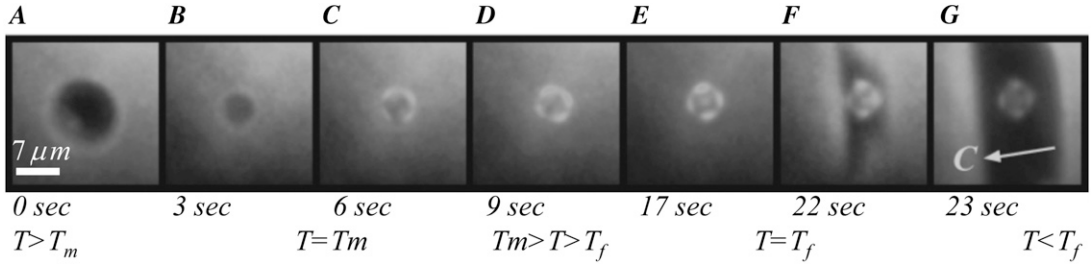

FIGURE 5 Melting and growth of an ice crystal in GFP-sbwAFP solution viewed by epifluorescence microscopy. (*A* and *B*) Melting of the ice crystal in the presence of GFP-sbwAFP. (*C–E*) Accumulation of GFP-sbwAFP on the surface of the ice crystal on cooling within the thermal hysteresis gap. (*F* and *G*) Rapid growth of the ice crystal when cooled below the nonequilibrium freezing point. The *c* axis is marked with a white arrow and is consistent for all the images displayed. Figures experimental time in sec (Movie S1 and Data S1). The temperature in this sequence changes from above the melting temperature ($T_m = -0.05°C$) to below the freezing temperature ($T_f \approx -1.0°C$).

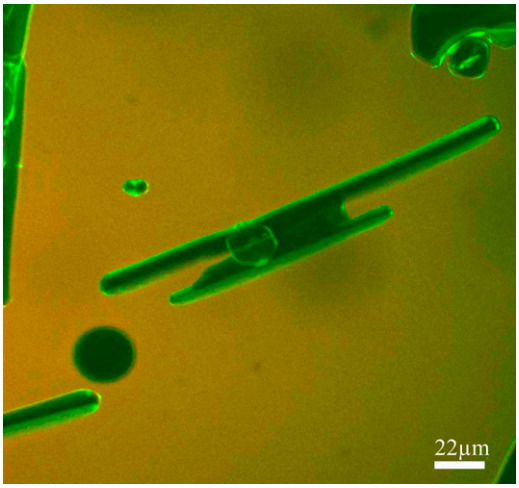

FIGURE 6 A confocal image of an ice crystal surrounded by GFP-sbwAFP after it has ''burst''. This lateral view shows the aftermath of the rapid expansion of the prism regions immediately under the two basal planes. The basal planes have enormously expanded in area and are highly fluorescent. The solution in this experiment contains in addition to the GFP-sbwAFP a second dye, Cy5, which does not interact with the ice and is confined to the solution. Imaging through both GFP and Cy5 filters results in orange color of the solution whereas the crystal decorated with GFP-sbwAFP is green (Movie S2).

the binding of these types of AFPs to ice crystals by fluorescence microscopy, and the results clearly show that the sbwAFP readily binds to the basal planes. Furthermore, mixtures of these two AFP types showed that the sbwAFP can bind to and stabilize the basal planes even in the presence of AFPIII, producing a truncated variant of the characteristic bipyramidal ice crystals formed in the presence of AFPIII alone.

In our visualization of ice crystals growing in the presence of GFP-sbwAFP alone, the symmetry of the distribution of fluorescence on the hexagonal shaped ice crystals clearly showed accumulation of the sbwAFP on two surfaces orthogonal to the axis of sixfold symmetry (the *c* axis), which are the basal planes. Additionally, we observed discrete patches of AFP at each of the six corners of the hexagon, which can be ascribed to binding to the residual primary prism plane surfaces that remain after partially melting the crystal (47). The flat surfaces that link these patches are oriented parallel to the secondary prism planes, which are perpendicular to the fastest melting direction. When the crystal was grown by lowering the temperature the six fluorescent patches became the centers of new primary prism planes that became evenly coated with the GFP-AFP. These surfaces, the slowest growing planes, have a 30° rotation from the apparent planes of the melting shape (47).

To observe GFP-AFPs bound to the surfaces of ice crystals, it is necessary to isolate single crystals floating in the solution containing antifreeze protein. This is readily achieved by snap freezing the entire sample by rapidly cooling to approximately −15°C, and then carefully melting it until only a small number of crystals of the desired size remain. It is interesting to note that in the presence of GFP-AFPIII, the core of these crystals contain large quantities of AFP, whereas, when crystals are formed in the presence of GFP-sbwAFP very little AFP becomes incorporated in these crystals. This result is consistent with observations of bursting ice crystals in the presence of each GFP-AFP fusion protein. AFPIII ice crystals burst as multiple spicules expanding in the *c*-axial direction that present a large surface area of prism planes to which AFPIII adsorbs before being engulfed. In the presence of sbwAFP, the hexagonal seed crystal appears to burst by growing laterally (orthogonal to the *c* axis) as a relatively smooth, single crystal. As this crystal expands, very little sbwAFP becomes engulfed. Surprisingly, the growing ice actively excludes much of the sbwAFP, which thus becomes concentrated ahead of the ice/liquid interface.

The exclusion of an AFP from a growing ice crystal might be explained by poor exposure of its binding plane(s) on the surface of the crystal, however this is not the case for sbwAFP as the surface of the growing ice crystal is bounded almost entirely by basal planes. The exclusion of sbwAFP is more likely related to the kinetics of its adsorption to the ice, i.e., the surface is growing too rapidly to allow sbwAFP to establish an attachment to ice. A video of a bursting ice

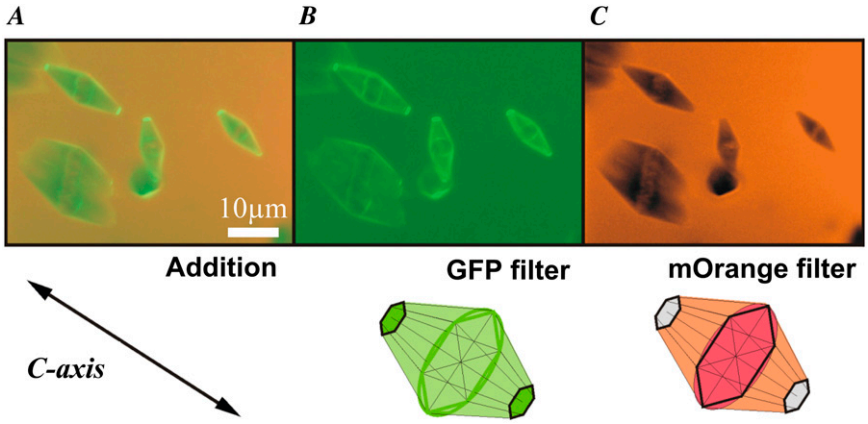

FIGURE 7 Ice crystals formed in the presence of a mixture of spruce budworm AFP and type III AFP Ice crystals produced in a solution containing both GFP-tagged sbwAFP and mOrange-labeled type III AFP, imaged with 488 nm and 543 nm illumination lines through two separate fluorescence filters of the confocal microscope: a GFP filter, and a mOrange filter. (*A*) Sum of the fluorescence contributions of the two fluorescent AFPs. (*B*) GFP-SbwAFP fluorescence alone. (*C*) mOrange-AFPIII fluorescence alone. Lower row: models of the ice crystal in the presence of the two fluorescent AFPs taken through GFP filter (*center*) and mOrange filter (*right*). At the left the arrow indicates the *c* axis of the models.

crystal (Movie S1 and Data S1) shows that the diameter of the prism planes grows rapidly and actively excludes the AFP. The basal plane of the bursting ice crystal appears to be well coated, although it is difficult to tell whether the AFP is concentrated in the liquid layer adjacent to this plane as a result of being excluded from ice. However, the basal plane grows so slowly compared to the prism plane that the overall engulfment of AFPs here would be low. In contrast, the spicules formed from bursting ice crystals in the presence of AFPIII grow rapidly parallel to the *c* axis but present a large surface area of slowly growing prism and pyramidal planes to which the AFPIII readily adsorbs.

In a previous study comparing the incorporation of different AFP types at low concentrations into slowly growing multicrystalline ice hemispheres, we found that fish and insect AFPs bind and become engulfed to a similar extent (52). This supports the notion that sbwAFP is excluded from bursting ice crystals because it fails to attach to the rapidly growing surface.

The idea that AFPs are capable of binding to the basal plane has been somewhat controversial. The basal plane is relatively 'smooth' on the atomic scale and thus grows slowly, whereas the prism plane is rough and grows more rapidly. The result of this discrepancy in growth rates is that ice crystals grown in water take on the shape of flat round discs (53). One explanation for why the basal plane is faceted whereas the prism plane is not is that three water molecules are needed to form a chain of hydrogen bonds between two water molecules on the basal plane whereas only two are needed on the prism plane (54,55). The greater number of water molecules involved in the hydrogen bonding chain on the basal plane gives rise to an entropic barrier to nucleation on this plane. Experimental observations have shown that although the basal plane is faceted, the prism plane is rough; hence no nucleation barrier exists under standard pressure on the prism plane. This difference in surface roughness may influence the ability of AFP molecules to lock onto the ice surface. One of the assumptions of the adsorption-inhibition theory for AFP activity is that the AFP molecules adsorb irreversibly on the ice surface (22,26). However, the concept of irreversibility has been challenged and is not accepted by all researchers. For instance, recent molecular dynamics simulation studies suggest that the energy involved in the interaction between type I AFP and ice is small, indicating that the interaction of the AFP molecule to the ice surface might not be long lasting (56). On the other hand, the adsorbed molecules might be stabilized due to the ice growth kinetics. It may be that the ability of the crystals to grow in all directions except the basal plane mediates growth around the bonded molecule, thereby locking it into the ice surface. On the basal plane, by contrast, this type of rapid lock-in mechanism would be less feasible due to the slow growth on this surface. In water containing AFPs with moderate antifreeze activity, the AFPs tend to block planes tilted toward the basal plane, leading to the formation of the typical bipyramidal ice shape in which the basal plane is reduced to a point at the apex of each pyramid. The unprotected basal plane represents a weak point in the protection of the crystal from freezing (33), as the basal plane can still grow even though it is faceted. When higher TH activity is required, such as in terrestrial organisms, the basal plane probably needs to be directly protected. It is still not clear if irreversible attachment occurs for the sbwAFP. In this work we see that a dynamic process is involved in the interaction between sbwAFP and ice. Moreover, we note that the accumulation of GFP-sbwAFP on the ice crystal occurs principally after growth is halted. This accumulation is not explained yet. It might indicate either on-surface growth or filling in of possible binding sites over time. This kind of accumulation was predicted in the work of Sander et al. (26). However, it is much more profound for sbwAFP than for AFPIII (4). It also might be that a combination of processes that include an irreversible binding of some of the molecules and reversible exchange of others is responsible for the phenomenon we observe. In addition, we note that when the sbwAFP molecules on a protected crystal are overgrown by new ice, many of them stay within the ice and become engulfed (Fig. 5, *F* and *G*, and Fig. 5 in Pertaya et al. (47)). This indicates that at least some molecules are irreversibly attached to the ice surface. Further investigation will determine if this dynamic process includes equilibrium exchange with the solution or other dynamic processes such as growth and rearrangement on a protected ice surface.

The results presented here clearly show that sbwAFP does adhere to the basal plane and are consistent with the results obtained by ice etching (39). It seems that the exquisite complementarity to the basal plane of the two-dimensional array of Thr residues found on the ice-binding face (39) is sufficient to mediate an energetically favorable attachment to this plane. The mechanism underlying such attachment might involve ice-lattice occupation via hydrogen bonding of the Thr hydroxyl group (43,44) or surface-surface complementarity (41).

Protection of the basal plane is common to all hyperactive AFPs studied to date, and has been proposed to be the mechanism that underlies their high activities (33). We have shown that sbwAFP protection of the basal plane is achieved by direct binding to this plane. It remains to be determined whether other hyperactive AFPs bind directly to the basal plane or prevent its growth by indirect mechanisms. For example, hyperactive flounder AFP (type I-hyp) produces a spindle-shaped ice crystal with sharp tips (34,36) and may prevent growth at the basal plane simply by minimizing the exposure of this plane at the crystal surface.

Fluorescently tagged AFPs are a valuable tool to help understand the mechanisms by which these diverse proteins inhibit ice growth. They allow the determination of the binding planes for an AFP using not only macroscopic ice hemispheres but also microscopic ice crystals bathed in AFP solution. Furthermore observation of microscopic ice crystals

shows the localization of AFPs as a crystal melts, grows, bursts or remains stable within the thermal hysteresis gap. Such information can shed light on the dynamics of antifreeze protein adsorption to the surface of the ice crystals.

SUPPLEMENTARY MATERIAL

To view all of the supplemental files associated with this article, visit www.biophysj.org.

We would like to thank Sherry Gauthier for preparing the GFP-sbwAFP and Dr. Rob Campbell for the structural images of GFP-tagged AFPs.

This work was supported by the Canadian Institutes for Health Research to P.L.D who holds a Canada Research Chair in Protein Engineering, the Condensed Matter and Surface Science program at Ohio University and the Biomimetic Nanoscience and Nanoscale Technology initiative at Ohio University to I.B.

REFERENCES

1. Davies, P. L., J. Baardsnes, M. J. Kuiper, and V. K. Walker. 2002. Structure and function of antifreeze proteins. *Philos. Trans. R. Soc. Lond. B Biol. Sci.* 357:927–935.
2. Yeh, Y., and R. E. Feeney. 1996. Antifreeze proteins: structures and mechanisms of function. *Chem. Rev.* 96:601–618.
3. Ewart, K. V., Q. Lin, and C. L. Hew. 1999. Structure, function and evolution of antifreeze proteins. *Cell. Mol. Life Sci.* 55:271–283.
4. Pertaya, N., C. B. Marshall, C. L. DiPrinzio, L. Wilen, E. Thomson, J. S. Wettlaufer, P. L. Davies, and I. Braslavsky. 2007. Fluorescence microscopy evidence for quasi-permanent attachment of antifreeze proteins to ice surfaces. *Biophys. J.* 92:3663–3674.
5. Cheng, C. H. C. 1998. Evolution of the diverse antifreeze proteins. *Curr. Opin. Genet. Dev.* 8:715–720.
6. Tomchaney, A. P., J. P. Morris, S. H. Kang, and J. G. Duman. 1982. Purification, composition, and physical properties of a thermal hysteresis ''antifreeze'' protein from larvae of the beetle, *Tenebrio molitor*. *Biochemistry.* 21:716–721.
7. Graham, L. A., and P. L. Davies. 2005. Glycine-rich antifreeze proteins from snow fleas. *Science.* 310:461.
8. Urrutia, M. E., J. G. Duman, and C. A. Knight. 1992. Plant thermal hysteresis proteins. *Biochim. Biophys. Acta.* 1121:199–206.
9. Worrall, D., L. Elias, D. Ashford, M. Smallwood, C. Sidebottom, P. Lillford, J. Telford, C. Holt, and D. Bowles. 1998. A carrot leucine-rich-repeat protein that inhibits ice recrystallization. *Science.* 282:115–117.
10. Gilbert, J. A., P. J. Hill, C. E. R. Dodd, and J. Laybourn-Parry. 2004. Demonstration of antifreeze protein activity in Antarctic lake bacteria. *Microbiology-SGM.* 150:171–180.
11. Muryoi, N., M. Sato, S. Kaneko, H. Kawahara, H. Obata, M. W. F. Yaish, M. Griffith, and B. R. Glick. 2004. Cloning and expression of afpA, a gene encoding an antifreeze protein from the arctic plant growth-promoting rhizobacterium Pseudomonas putida GR12–2. *J. Bacteriol.* 186:5661–5671.
12. Robinson, C. H. 2001. Cold adaptation in Arctic and Antarctic fungi. *New Phytol.* 151:341–353.
13. Huang, T., J. Nicodemus, D. G. Zarka, M. F. Thomashow, M. Wisniewski, and J. G. Duman. 2002. Expression of an insect (*Dendroides canadensis*) antifreeze protein in *Arabidopsis thaliana* results in a decrease in plant freezing temperature. *Plant Mol. Biol.* 50:333–344.
14. Khanna, H. K. and G. E. Daggard. 2006. Targeted expression of redesigned and codon optimised synthetic gene leads to recrystallisation inhibition and reduced electrolyte leakage in spring wheat at sub-zero temperatures. *Plant Cell Rep.* 25:1336–1346.
15. Griffith, M., and K. V. Ewart. 1995. Antifreeze proteins and their potential use in frozen foods. *Biotechnol. Adv.* 13:375–402.
16. Breton, G., J. Danyluk, F. Ouellet, and F. Sarhan. 2000. Biotechnological applications of plant freezing associated proteins. *Biotechnol. Annu. Rev.* 6:59–101.
17. Rubinsky, B., A. Arav, and A. L. Devries. 1992. The cryoprotective effect of antifreeze glycopeptides from Antarctic fishes. *Cryobiology.* 29:69–79.
18. Li, B., and D. W. Sun. 2002. Novel methods for rapid freezing and thawing of foods—a review. *J. Food Eng.* 54:175–182.
19. Hew, C., R. Poon, F. Xiong, S. Gauthier, M. Shears, M. King, P. Davies, and G. Fletcher. 1999. Liver-specific and seasonal expression of transgenic Atlantic salmon harboring the winter flounder antifreeze protein gene. *Transgenic Res.* 8:405–414.
20. Raymond, J. A., and A. L. DeVries. 1977. Adsorption inhibition as a mechanism of freezing resistance in polar fishes. *Proc. Natl. Acad. Sci. USA.* 74:2589–2593.
21. Knight, C. A. 2000. Structural biology: adding to the antifreeze agenda. *Nature.* 406:249–251.
22. Knight, C. A., and A. Wierzbicki. 2001. Adsorption of biomolecules to ice and their effects upon ice growth. 2. A discussion of the basic mechanism of ''antifreeze'' phenomena. *Cryst. Growth Des.* 1:439–446.
23. Sonnichsen, F. D., C. I. DeLuca, P. L. Davies, and B. D. Sykes. 1996. Refined solution structure of type III antifreeze protein: hydrophobic groups may be involved in the energetics of the protein-ice interaction. *Structure.* 4:1325–1337.
24. Harding, M. M., L. G. Ward, and A. D. Haymet. 1999. Type I 'antifreeze' proteins. Structure-activity studies and mechanisms of ice growth inhibition. *Eur. J. Biochem.* 264:653–665.
25. Yang, D. S., W. C. Hon, S. Bubanko, Y. Xue, J. Seetharaman, C. L. Hew, and F. Sicheri. 1998. Identification of the ice-binding surface on a type III antifreeze protein with a ''flatness function'' algorithm. *Biophys. J.* 74:2142–2151.
26. Sander, L. M., and A. V. Tkachenko. 2004. Kinetic pinning and biological antifreezes. *Phys. Rev. Lett.* 93:128102.
27. Knight, C. A., A. L. DeVries, and L. D. Oolman. 1984. Fish antifreeze protein and the freezing and recrystallization of ice. *Nature.* 308:295–296.
28. Knight, C. A., C. C. Cheng, and A. L. DeVries. 1991. Adsorption of alpha-helical antifreeze peptides on specific ice crystal surface planes. *Biophys. J.* 59:409–418.
29. DeLuca, C. I., H. Chao, F. D. Sonnichsen, B. D. Sykes, and P. L. Davies. 1996. Effect of type III antifreeze protein dilution and mutation on the growth inhibition of ice. *Biophys. J.* 71:2346–2355.
30. Antson, A. A., D. J. Smith, D. I. Roper, S. Lewis, L. S. D. Caves, C. S. Verma, S. L. Buckley, P. J. Lillford, and R. E. Hubbard. 2001. Understanding the mechanism of ice binding by type III antifreeze proteins. *J. Mol. Biol.* 305:875–889.
31. Graham, L. A., Y. C. Liou, V. K. Walker, and P. L. Davies. 1997. Hyperactive antifreeze protein from beetles. *Nature.* 388:727–728.
32. Tyshenko, M. G., D. Doucet, P. L. Davies, and V. K. Walker. 1997. The antifreeze potential of the spruce budworm thermal hysteresis protein. *Nat. Biotechnol.* 15:887–890.
33. Scotter, A. J., C. B. Marshall, L. A. Graham, J. A. Gilbert, C. P. Garnham, and P. L. Davies. 2006. The basis for hyperactivity of antifreeze proteins. *Cryobiology.* 53:229–239.
34. Marshall, C. B., G. L. Fletcher, and P. L. Davies. 2004. Hyperactive antifreeze protein in a fish. *Nature.* 429:153.
35. Gauthier, S. Y., C. B. Marshall, G. L. Fletcher, and P. L. Davies. 2005. Hyperactive antifreeze protein in flounder species. *FEBS J.* 272:4439–4449.
36. Marshall, C. B., A. Chakrabartty, and P. L. Davies. 2005. Hyperactive antifreeze protein from winter flounder is a very long rod-like dimer of alpha-helices. *J. Biol. Chem.* 280:17920–17929.
37. Gilbert, J. A., P. L. Davies, and J. Laybourn-Parry. 2005. A hyperactive, Ca^{2+}-dependent antifreeze protein in an Antarctic bacterium. *FEMS Microbiol. Lett.* 245:67–72.

38. Gauthier, S. Y., C. M. Kay, B. D. Sykes, V. K. Walker, and P. L. Davies. 1998. Disulfide bond mapping and structural characterization of spruce budworm antifreeze protein. *Eur. J. Biochem.* 258:445–453.

39. Graether, S. P., M. J. Kuiper, S. M. Gagne, V. K. Walker, Z. Jia, B. D. Sykes, and P. L. Davies. 2000. Beta-helix structure and ice-binding properties of a hyperactive antifreeze protein from an insect. *Nature.* 406:325–328.

40. Leinala, E. K., P. L. Davies, and Z. C. Jia. 2002. Crystal structure of beta-helical antifreeze protein points to a general ice binding model. *Structure.* 10:619–627.

41. Leinala, E. K., P. L. Davies, D. Doucet, M. G. Tyshenko, V. K. Walker, and Z. Jia. 2002. A beta-helical antifreeze protein isoform with increased activity. Structural and functional insights. *J. Biol. Chem.* 277:33349–33352.

42. Knight, C. A., E. Driggers, and A. L. Devries. 1993. Adsorption to ice of fish antifreeze glycopeptide-7 and glycopeptide-8. *Biophys. J.* 64:252–259.

43. Liou, Y. C., A. Tocilj, P. L. Davies, and Z. C. Jia. 2000. Mimicry of ice structure by surface hydroxyls and water of a beta-helix antifreeze protein. *Nature.* 406:322–324.

44. Bar, M., Y. Celik, D. Fass, and I. Braslavsky. 2008. Interactions of β-helical antifreeze protein mutants with Ice. *Crystal Growth & Design.* In press.

45. Jia, Z. C., C. I. DeLuca, H. M. Chao, and P. L. Davies. 1996. Structural basis for the binding of a globular antifreeze protein to ice. *Nature.* 384:285–288.

46. Iyer, L. M., and L. Aravind. 2004. The emergence of catalytic and structural diversity within the beta-clip fold. *Proteins.* 55:977–991.

47. Pertaya, N., Y. Celik, C. L. Di Prinzio, J. Wettlaufer, P. L. Davies, and I. Braslavsky. 2007. Growth-melt asymmetry in ice crystals under the influence of spruce budworm antifreeze protein. *J. Phys. Condens. Matter.* 19:412101.

48. Heim, R., A. B. Cubitt, and R. Y. Tsien. 1995. Improved green fluorescence. *Nature.* 373:663–664.

49. Shaner, N. C., R. E. Campbell, P. A. Steinbach, B. N. G. Giepmans, A. E. Palmer, and R. Y. Tsien. 2004. Improved monomeric red, orange and yellow fluorescent proteins derived from *Discosoma sp* red fluorescent protein. *Nat. Biotechnol.* 22:1567–1572.

50. Kuiper, M. J., C. Lankin, S. Y. Gauthier, V. K. Walker, and P. L. Davies. 2003. Purification of antifreeze proteins by adsorption to ice. *Biochem. Biophys. Res. Commun.* 300:645–648.

51. DeLuca, C. I., R. Comley, and P. L. Davies. 1998. Antifreeze proteins bind independently to ice. *Biophys. J.* 74:1502–1508.

52. Marshall, C. B., M. M. Tomczak, S. Y. Gauthier, M. J. Kuiper, C. Lankin, V. K. Walker, and P. L. Davies. 2004. Partitioning of fish and insect antifreeze proteins into ice suggests they bind with comparable affinity. *Biochemistry.* 43:148–154.

53. Shimada, W., and Y. Furukawa. 1997. Pattern formation of ice crystals during free growth in supercooled water. *J. Phys. Chem. B.* 101:6171–6173.

54. Jackson, K. A., D. R. Uhlmann, and J. D. Hunt. 1967. On the nature of crystal growth from the melt. *J. Crystal Growth.* 1:1–36.

55. Braslavsky, I. 1998. Imaging of the temperature field around a dendritic crystal. PhD dissertation. Technion, Haifa, Israel.

56. Wierzbicki, A., P. Dalal, T. E. Cheatham, J. E. Knickelbein, A. D. J. Haymet, and J. D. Madura. 2007. Antifreeze proteins at the Ice/Water interface: three calculated discriminating properties for orientation of type I proteins. *Biophys. J.* 93:1442–1451.